Theoretical Chemistry Accounts (2018) 137:130
https://doi.org/10.1007/s00214-018-2320-2

REGULAR ARTICLE

Unveiling the effects of doping small nickel clusters with a sulfur impurity

Abdelaziz Chikhaoui[1] · Mohamed Ziane[1] · Slimane Tazibt[1] · Said Bouarab[1] · Andrés Vega[2]

Received: 19 March 2018 / Accepted: 25 September 2018 / Published online: 4 October 2018

Abstract
Small free-standing Ni clusters have been widely investigated during the last decade, but not many of their derived chalcogenides, despite their interest in technology and the new prospects that the nanoscale may open. The present work uncovers the effects of the S-doping on the structural, electronic, and magnetic properties of Ni_n, $n = 1$–10 clusters. Density functional theoretical calculations within the generalized gradient approximation for the exchange and correlation were conducted to explore the structural, electronic, and magnetic properties of the resulting Ni_nS chalcogenide nanoparticles. The sulfur impurity is always adsorbed on the threefold hollow sites available on the nickel host, in qualitative agreement with recent results of S adsorption on Ni(111) surfaces. S-doping tends to enlarge the average Ni–Ni inter-atomic distance but enhances the thermodynamical stability of Ni clusters. It also increases the vertical ionization energy and electron affinity. However, S-doping has a small effect on the magnetism of small Ni clusters. According to the spin-dependent HOMO–LUMO gap, most of these clusters are good candidates as molecular junctions for spin filtering at low bias voltage.

Keywords Ab initio calculations · Doping · Electronic properties · Magnetic properties · Nickel · Sulfur

1 Introduction

The chalcogenides are an important class of materials from the technological viewpoint due to their significant electrical, optical, and chemical characteristics. The applications of chalcogenide materials include a variety of chalcogenide glasses, infrared sensors, solar energy conversion, and window layer [1–6]. Among chalcogenide nanomaterials, nickel sulfide NiS presents potential applications in photoconduction [7]. In general, sulfur compounds such as transition metal sulfides have important applications in superconduction [8, 9], biochemical systems [10, 11], and catalysis [12–14]. As thin films and at the nanoscale, the chalcogenides as it happens with most materials present a wide range of new properties inherent to the quantum confinement, which deserve to be explored by the Scientific Community. The main characteristic of nanomaterials comes from the sensitivity of their electronic properties with their morphologies, size, and composition that can be completely different from their mesoscopic and macroscopic counterparts, thus offering new prospects for developing a wide range of new applications.

Small free-standing Ni clusters have been widely investigated from different theoretical approaches [15–43] and experimentally [44, 45] during nearly two decades. However, no studies have been carried out so far regarding the effects of doping small nickel clusters with a light impurity. Oxygen and sulfur impurities are particularly interesting in this context, due to their abundance, their different electronegativity as compared with Ni, and the relevance of nickel oxide and chalcogenides. By doping the pure Ni_n clusters with an electronegative element like sulfur, local charge transfer is expected which could induce a partial ionic contribution to the local bonding in the system. The aim of the present work is to perform a systematic theoretical study of the evolution of the structural, electronic, and magnetic properties of small Ni clusters when doped with a single sulfur impurity. We performed density functional theoretical calculations of Ni_nS clusters in the size range of $n = 1$–10.

✉ Abdelaziz Chikhaoui
aziz_chikhawi@yahoo.fr

[1] Laboratoire de Physique et Chimie Quantique, Faculté des Sciences, Université Mouloud Mammeri de Tizi-Ouzou, B.P. No. 17 RP, 15000 Tizi-Ouzou, Algeria

[2] Departamento de Física Teórica, Atómica y Óptica, Universidad de Valladolid, Paseo Belén 7, 47011 Valladolid, Spain

We determined the most stable atomic arrangements, the absolute and relative stabilities, the electronic structure and magnetic properties, and electronic indicators such as ionization potentials and electron affinities.

A description of our theoretical approach is done in the next section. The results are presented in Sect. 3 in which we first present the structural properties and then we discuss the stability and electronic properties. The main conclusions are summarized at the end.

2 Computational method

Calculations were conducted within the density functional theory, using a plane wave basis set and the projected augmented wave (PAW) approach for the core interactions, as implemented in the VASP code [46]. We considered the $3d^8 4s^2$ valence configuration for Ni, and $3s^2 3p^4$ for S. A plane wave energy cutoff of 300 eV was taken. The exchange and correlation effects were treated in the generalized gradient approximation (GGA) by using the Perdew–Burke–Ernzerhof functional [47]. A cubic supercell with lateral size of 15 Å was employed for all the calculations. Only the Γ point was taken for integrations in the Brillouin zone. The cluster geometry was optimized, without symmetry constraints, until the force on each atom was less than 0.001 eV/Å, and the total energy was converged to 10^{-6} eV. For charged clusters, corrections to the total energy were included by considering the full dipole moment in all directions. The corrections were calculated as the energy difference between a monopole, dipole, or quadrupole in the current supercell and the same monopole, dipole, or quadrupole placed in a vacuum. Furthermore, the quadrupole corrections originating from the expectation value of r^2 were also taken into account.

The lowest-energy structures of pure Ni_n clusters were obtained by considering various initial configurations with different symmetries. Most of the inputs used were taken from previously published works. For doped Ni_nS clusters, we considered various initial atomic arrangements with the S atom occupying the different sites, and also by adsorbing it on all possible sites of several bare Ni_n low-lying isomers (first, second, and sometimes third isomers) calculated beforehand. We checked that the results remain unchanged after small displacements of the atoms around their equilibrium positions and also for higher cutoff energies and even more stringent convergence criteria. The relative stability of different isomers was further checked by performing calculations in different spin states to be sure of the total spin of the putative ground state. Although we did not employ an unbiased structural search, we believe that our sampling should be sufficient due to the small size of the clusters.

With the VASP code, the local charges and spin magnetic moments are computed by projecting the plane wave components of the eigenstates onto spherical waves inside slightly overlapping atomic spheres of Wigner–Seitz radius. Because this projection depends on the choice of the atomic radius, the sum of the local charges and moments is not necessarily and always identical to the total cluster values. In order to overcome this issue when analyzing the local magnetic moments distribution, we performed the analysis by using Bader's method [48–50] which is based on partitioning the cluster into atomic volumes by locating the zero-flux surfaces of the electron density field.

The accuracy of the calculation method is checked by comparing the calculated bond length, vibration frequency, ionization potential, and electronic affinity of both Ni_2 and S_2 dimers, with available experimental data. The results for Ni_2, summarized in Table 1, show a fairly good agreement between the calculated and the measured values of the different quantities considered. As for the calculations for S_2, the consistency of the results with the experimental data can be found in our previous paper on Fe_nS_2 clusters [51]. Moreover, additional test calculations for hexagonal bulk NiS (NiAs structure) give lattice parameters of 3.45 and 5.20 Å in good agreement with the measured values of 3.44 and 5.32 Å [52].

3 Results and discussion

3.1 Structural properties

In order to extract conclusions about the effect of S-doping on the structural and electronic properties, we have first determined the putative ground state of the corresponding pure Ni_n clusters which we also compare with previous results available in the literature. The atomic configurations adopted by the putative minimum energy structure of Ni_n and Ni_nS (n = 1–10) clusters are displayed in Figs. 1 and 2. Only the geometries of the putative ground state are described along the text, except if certain isomers are energetically competitive with the ground state. Information

Table 1 Calculated values of bond length r, vibrational frequency ω, ionization potential IP, and electronic affinity EA for Ni_2 dimer, compared to experimental data

Ni_2 dimer	r (Å)	ω (cm^{-1})	IP (eV)	EA (eV)
This work	2.09	320	7.91	1.0
Exp. works	(2.15)[a]	259.2 ± 3.0[b]	7.65[c]	0.93[d]
		381[e]		

[a] [53],[b] [54],[c] [44],[d] [45],[e] [55]

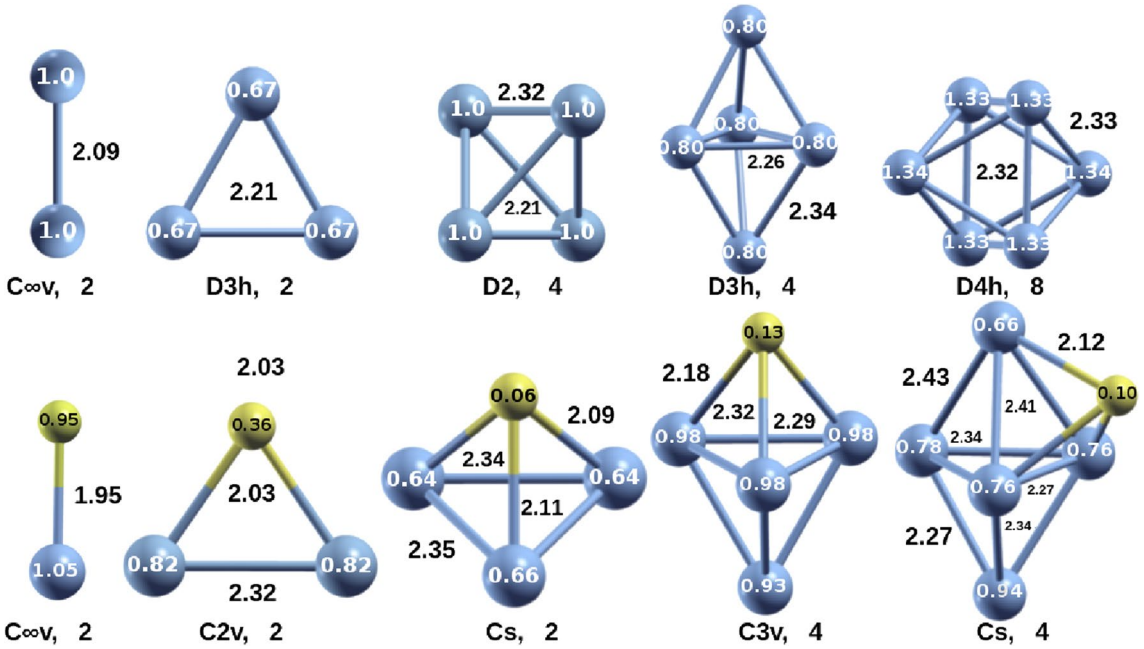

Fig. 1 Putative ground-state structures of Ni_n, n = 2–6 (first line) and Ni_nS, n =1–5 (second line) clusters, with their corresponding point-group symmetry and total magnetic moment (μ_B). Bond lengths are given in Å and the local spin moments are given (in μ_B) inside the atomic spheres

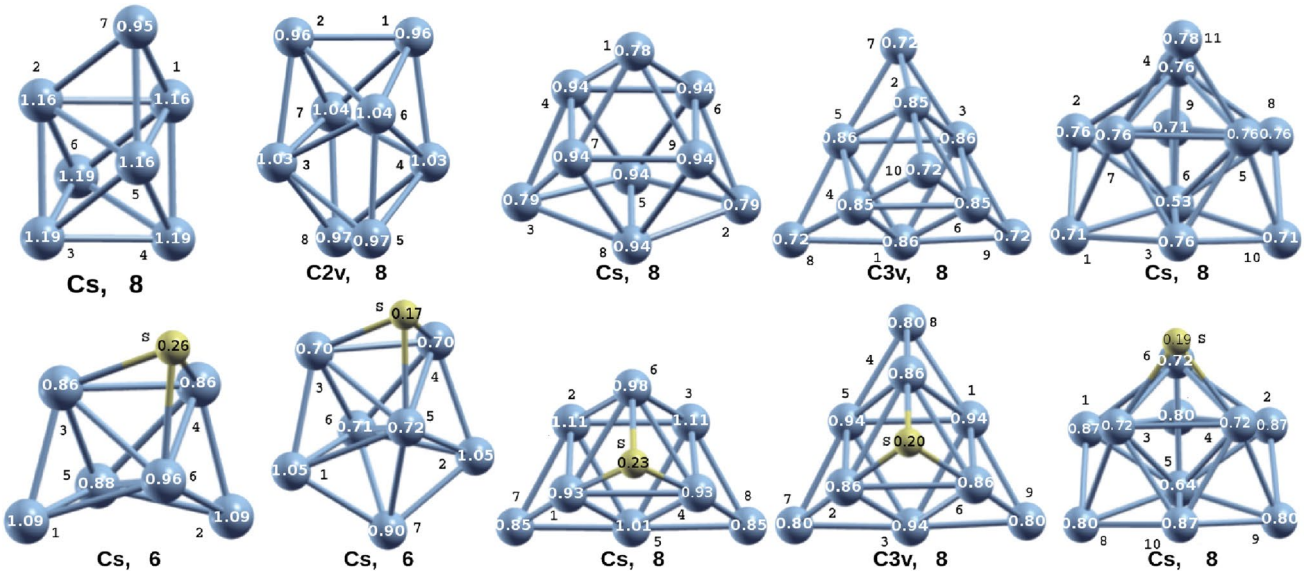

Fig. 2 Putative ground-state structures of Ni_n (n = 7–11) and Ni_nS (n = 6–10) clusters, with their corresponding point-group symmetry and total magnetic moment (μ_B). The local spin moments are given (in μ_B) inside the atomic spheres, whereas the bond lengths are given in Table 2 according to the labels of the different atoms

about all the low-lying isomers found in the present work can be obtained from the authors upon request.

3.1.1 Ni_n clusters

We note that neutral Ni_n clusters have been the subject of several theoretical studies [15–30, 32–37, 39–43] against which we can benchmark our theoretical approach. Let us note that our group already performed DFT calculations [43]

Table 2 Inter-atomic distances r_{ij} (Å) in Ni_n, $n = 7$–11 clusters according to the labels of the different atoms of Fig. 2

Ni_7	Ni_8	Ni_9	Ni_{10}	Ni_{11}
$r_{12} = r_{25} = r_{51} = 2.32$	$rr_{16} = r_{26} = 2.36$	$r_{14} = r_{16} = r_{17} = r_{19} = 2.37$	$r_{15} = r_{35} = r_{31} = 2.41$	$r_{12} = r_{13} = 2.37$
$r_{34} = r_{46} = r_{63} = 2.32$	$r_{17} = r_{27} = 2.35$	$r_{26} = r_{29} = r_{34} = r_{37} = 2.37$	$r_{26} = r_{46} = r_{24} = 2.42$	$r_{24} = r_{35} = 2.38$
$r_{14} = r_{45} = r_{35} = 2.35$	$r_{14} = r_{23} = 2.37$	$r_{25} = r_{28} = r_{35} = r_{38} = 2.36$	$r_{27} = r_{48} = r_{69} = 2.28$	$r_{45} = 2.43$
$r_{32} = r_{26} = r_{16} = 2.35$	$r_{36} = r_{46} = 2.28$	$r_{45} = r_{65} = r_{78} = r_{98} = 2.35$	$r_{37} = r_{57} = r_{39} = 2.28$	$r_{26} = r_{36} = 2.31$
$r_{17} = r_{27} = r_{57} = 2.32$	$r_{35} = r_{45} = 2.37$	$r_{46} = r_{79} = 2.36$	$r_{19} = r_{18} = r_{58} = 2.28$	$r_{46} = r_{56} = 2.60$
	$r_{38} = r_{48} = 2.36$	$r_{47} = r_{69} = 2.24$	$r_{14} = r_{16} = r_{32} = 2.41$	$r_{16} = 2.33$
	$r_{37} = r_{47} = 2.29$	$r_{85} = 2.32$	$r_{36} = r_{52} = r_{54} = 2.41$	$r_{27} = r_{37} = 2.38$
	$r_{58} = 2.32$			$r_{47} = r_{57} = 2.42$
	$r_{12} = 2.34$			$r_{17} = 2.32$
				$r_{48} = r_{58} = 2.38$
				$r_{67} = 2.59$
				$r_{68} = 2.31$
				$r_{411} = r_{511} = 2.28$
				$r_{711} = 2.28$
				$r_{92} = r_{103} = 2.37$
				$r_{94} = r_{105} = 2.32$
				$r_{96} = r_{106} = 2.37$
				$r_{98} = r_{108} = 2.36$

for pure Ni clusters by using the SIESTA code [56, 57] with the same approximation for exchange and correlation (GGA–PBE) as in the present work. This method is based on norm-conserving pseudopotentials and linear combinations of atomic orbitals as basis sets for which we used triple-ζ with double polarization functions. In general, our present results for nickel clusters are similar to those previously obtained with the SIESTA code [43]. There exist nevertheless some exceptions like Ni_5 for which VASP gives a trigonal bipyramid of D_{3h} symmetry and total moment of 4 μ_B, whereas SIESTA gave a square pyramid of C_{4v} symmetry and 6 μ_B of total moment. However, we point out that the first isomer of Ni_5 with total moment of 6 μ_B is found at only 0.03 eV of energy above the putative ground state with total moment of 4 μ_B. Apart from slight relaxations, our optimized geometries of neutral Ni_n clusters, displayed in Figs. 1 and 2, are also consistent with previous results published elsewhere, except for few sizes in which a similar scenario as in the previously mentioned case of Ni_5 in the SIESTA versus VASP benchmark occurs. Different approaches at the DFT level are known to give rise sometimes to slightly different energetic ordering of the low-lying isomers. It is for this reason that recalculating the pure Ni clusters at the same level of accuracy as the S-doped clusters is appealing for providing a consistent analysis (Table 3).

3.1.2 Ni_nS clusters

We discuss first the general trends. We find that the S atom tends to occupy a threefold hollow site on the Ni_n host clusters, in qualitative agreement with recent DFT calculations [58] where it was shown that the sulfur adsorption on the Ni(100) and Ni(110) surfaces takes preferably place on the most coordinated sites.

The computed average Ni–Ni distance (AD) in both Ni_n and Ni_nS clusters is plotted as a function of cluster size n in Fig. 3a. In pure nickel clusters, it increases up to $n = 5$ and then it keeps nearly constant to stabilize around a value of 2.35 Å. The situation is different in the S-doped clusters, where the Ni–Ni distance increases with respect to that of the pure Ni_n clusters although with a lower slope. Let us now analyze in some detail the structures of the different clusters.

The ground state of Ni_2S is an isosceles triangle (C_{2v} symmetry), with Ni–S and Ni–Ni bond lengths of 2.03 and 2.32 Å, respectively. Its total magnetic moment of 2μ_B results from a parallel magnetic coupling between the Ni atoms ($2 \times 0.82\ \mu_B$) and the S atom (0.36 μ_B). We note that S-doping considerably enhances the Ni–Ni bond length, as in the pure Ni_3 (D_{3h}) these bond lengths are 2.21 Å, and even smaller in Ni_2 (2.09 Å), both pure clusters having also 2μ_B.

For Ni_3S, the putative ground state is a trigonal pyramid of C_s symmetry and total moment of 2 μ_B, as that of Ni_3. The local moments on Ni atoms are 2×0.64 and 0.66 μ_B whereas the induced moment on S is very small 0.06 μ_B. A trigonal pyramid of C_{3v} is the first isomer, lying at just 0.02 eV above the ground state. The pure Ni_4 is a tetrahedron (D_2) with total moment of 4 μ_B. In this case, substitutional doping reduces the total magnetic moment. Doping also enhances the average Ni–Ni inter-atomic distance.

Table 3 Inter-atomic distances r_{ij} (Å) in Ni_nS, $n = 6$–10 clusters according to the labels of the different atoms of Fig. 2

Ni_6S	Ni_7S	Ni_8S	Ni_9S	$Ni_{10}S$
$r_{13} = r_{24} = 2.29$	$r_{17} = r_{27} = 2.32$	$r_{15} = r_{45} = 2.42$	$r_{15} = r_{13} = r_{35} = 2.42$	$r_{17} = r_{27} = 2.37$
$r_{36} = r_{46} = 2.33$	$r_{13} = r_{24} = 2.38$	$r_{25} = r_{35} = 2.38$	$r_{24} = r_{46} = r_{62} = 2.54$	$r_{13} = r_{24} = 2.40$
$r_{15} = r_{25} = 2.27$	$r_{15} = r_{25} = 2.42$	$r_{12} = r_{34} = 2.34$	$r_{19} = r_{39} = r_{37} = 2.28$	$r_{15} = r_{25} = 2.29$
$r_{3S} = r_{4S} = 2.15$	$r_{35} = r_{45} = 2.39$	$r_{16} = r_{46} = 2.42$	$r_{75} = r_{85} = r_{81} = 2.28$	$r_{35} = r_{45} = 2.64$
$r_{35} = r_{45} = 2.42$	$r_{16} = r_{26} = 2.36$	$r_{26} = r_{36} = 2.36$	$r_{27} = r_{69} = r_{48} = 2.31$	$r_{18} = r_{29} = 2.36$
$r_{16} = r_{26} = 2.38$	$r_{36} = r_{46} = 2.38$	$r_{17} = r_{48} = 2.31$	$r_{2S} = r_{4S} = r_{6S} = 2.16$	$r_{85} = r_{95} = 2.34$
$r_{34} = 2.15$	$r_{3S} = r_{4S} = 2.13$	$r_{27} = r_{38} = 2.31$		$r_{38} = r_{49} = 2.34$
$r_{65} = 2.43$	$r_{34} = 2.53$	$r_{57} = r_{58} = 2.29$		$r_{310} = r_{410} = 2.40$
$r_{6S} = 2.24$	$r_{57} = 2.37$	$r_{1S} = r_{4S} = 2.18$		$r_{810} = r_{910} = 2.37$
	$r_{56} = 2.47$	$r_{14} = 2.54$		$r_{16} = r_{26} = 2.40$
	$r_{56} = 2.47$	$r_{23} = 2.35$		$r_{16} = r_{26} = 2.40$
	$r_{67} = 2.28$	$r_{6S} = 2.19$		$r_{36} = r_{46} = 2.50$
	$r_{5S} = 2.20$			$r_{3S} = r_{4S} = 2.16$
				$r_{34} = 2.50$
				$r_{76} = 2.34$
				$r_{6S} = 2.16$
				$r_{57} = 2.34$
				$r_{510} = 2.29$

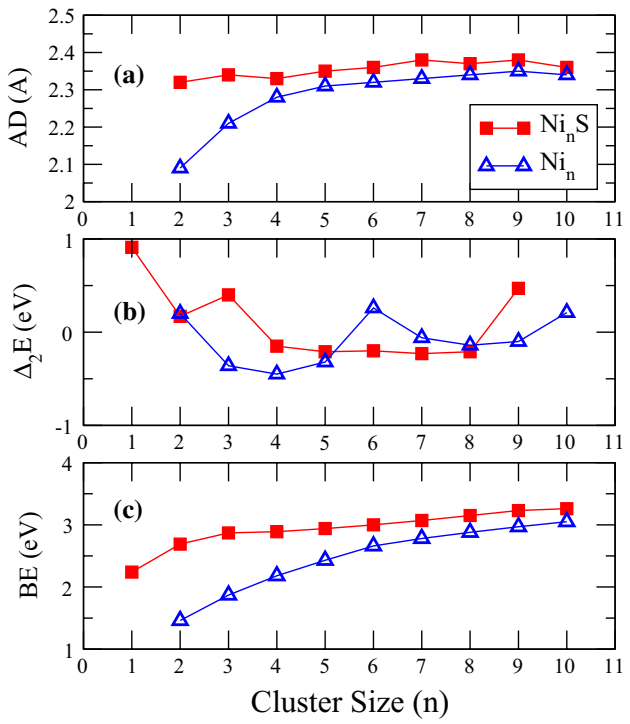

Fig. 3 **a** Calculated average Ni–Ni distance (AD), **b** second energy difference ($\Delta_2 E$), and **c** binding energy (BE) as function of cluster size n =1–10

Ni_4S is a trigonal bipyramid of C_{3v} symmetry and 4 μ_B of total moment. The two non-equivalent Ni–Ni bond lengths (2.32 and 2.29 Å) are slightly larger than those of Ni–S bonds (2.18 Å). The local Ni moments are 3×0.98 and 0.93 μ_B whereas the S atom is noticeably polarized (0.13 μ_B). The same atomic arrangement, but with a C_s symmetry and the same total moment (4 μ_B) is found as the first isomer at only 0.01 eV above. The pure Ni_5 is a trigonal bipyramid of D_{3h} symmetry and total moment of 4 μ_B, meaning that doping here does not modify the magnetic moment.

The putative lowest-energy structure of Ni_5S is a Ni_5 distorted trigonal pyramid capped by the S atom on one of its threefold hollow sites. It has C_s symmetry and a total moment of 4 μ_B. The pure Ni_6 cluster is a square bipyramid of D_{4h} symmetry and 8 μ_B of total moment resulting from the distribution of the moments of the base atoms (4×1.33 μ_B) and the apex atoms (2×1.34 μ_B). This Ni_6 structure with D_{4h} symmetry is energetically quasi-degenerated ($\Delta E = 0.01$ eV) with the same atomic arrangement having C_i symmetry. Substitutional doping reduces the total moment and leads to an important atomic rearrangement.

For Ni_6S, the putative ground state is obtained from the Ni_6 square bipyramid where the S atom is adsorbed on a threefold hollow site giving rise to a Ni–Ni bond breaking on the base. It has C_s symmetry and a moment of 6 μ_B. A similar atomic arrangement but with C_{3v} symmetry and the same total magnetic moment as pure Ni_6 (8 μ_B), is found as the first isomer at only 0.04 eV above. The Ni_7 cluster is an Ni_6 octahedron capped by the seventh Ni atom on one of its threefold hollow site. It is of C_s symmetry and bears a total moment of 8 μ_B. As expected, the effect of enlarging the average Ni–Ni inter-atomic distance upon S-doping decreases as increasing the size of the Ni cluster.

The putative lowest-energy structure of Ni_7S is a distorted pentagonal bipyramid of C_s symmetry where the S atom

caps one of its threefold hollow sites. It bears a total moment of 6 μ_B. The reduction of the magnetic moment of the host cluster upon S-doping (by 2 μ_B) that takes place for Ni_7S as well as for Ni_6S is less marked than for the smaller clusters discussed above; for larger clusters, as we will see, this effect disappears. We will come later to this point when discussing the electronic properties. Ni_8 has a bisdisphenoid configuration with C_{2v} symmetry and total magnetic moment of 8 μ_B.

Ni_8S is a Ni_6 octahedron capped by two Ni and one S atoms on threefold hollow sites. It has C_s symmetry and total moment of 8 μ_B. The putative lowest-energy structure of Ni_9 is a trigonal prism tricapped of C_{2v} symmetry and total moment of 8 μ_B.

The putative ground state of Ni_9S is an octahedron Ni_6 capped by three Ni atoms and the S atom, on threefold hollow sites. It has the same symmetry (C_{3v}) and same total moment (8 μ_B) as the putative lowest-energy structure of Ni_{10} where one of the Ni atoms is replaced by S (Fig. 2).

Finally, the lowest-energy structure of $Ni_{10}S$ is a distorted pentagonal bipyramid of C_s symmetry and total moment of 8 μ_B, capped by three Ni atoms on threefold hollow sites. It was obtained by substituting the tenth atom of the Ni_{11} cluster by the S atom (Fig. 2).

3.2 Stability and electronic properties

The binding energies (BEs) per atom for both Ni_n and Ni_nS clusters (n =1–10) are plotted in Fig. 3c. BE is calculated from the following expressions

$$\mathrm{BE(Ni}_n) = [-E(\mathrm{Ni}_n) + nE(\mathrm{Ni})]/n, \quad (1)$$

$$\mathrm{BE(Ni}_n\mathrm{S}) = [-E(\mathrm{Ni}_n\mathrm{S}) + nE(\mathrm{Ni}) + E(S)]/(n+1). \quad (2)$$

First, we notice that the general behavior of the BE of pure Ni_n clusters as function of size is consistent with previous theoretical results [26, 27, 32, 36, 39, 42, 43]. BEs of Ni_nS clusters are larger than those of pure Ni_n, particularly for the smallest sizes for which the Ni/S rate is larger. As expected, BEs of pure and doped clusters tend to converge to each other as increasing cluster size. This reflects the obvious fact that a single S atom is averaged with an increasing number of Ni atoms. For clusters larger than those investigated here, it is expected that the S atom will continue to occupy preferentially the most coordinated hollow sites, as it occurs in surfaces [58], with concomitant local relaxations but without affecting the rest of the host cluster. The binding energy indicates that S-doping enhances the thermodynamical stability of the Ni clusters. This binding increase is related to the strong S–Ni bonding, reflected in the kind of adsorption site (the S atom is bonded with three Ni atoms in a threefold hollow site). As we will see later, the strong S–Ni bond is favored by a partial ionic contribution due to charge transfer from Ni to S as a consequence of the different electronegativities of the two elements (S is more electronegative than Ni).

A further evidence of the strong S–Ni bonding is provided by the single-atom fragmentation energies. We considered two single-atom fragmentation channels of Ni_nS, involving one Ni atom or the S atom. These quantities, plotted in Fig. 4a, are defined in terms of total energies as follows:

$$\Delta_S = E[\mathrm{Ni}_n] + E[\mathrm{S}] - E[\mathrm{Ni}_n\mathrm{S}], \quad (3)$$

$$\Delta_{\mathrm{Ni}} = E[\mathrm{Ni}_{n-1}\mathrm{S}] + E[\mathrm{Ni}] - E[\mathrm{Ni}_n\mathrm{S}]. \quad (4)$$

One can see from Fig. 4a that Δ_S is larger than Δ_{Ni}, for any size n, showing that the desulfurization (removing the S atom) of Ni_nS systems requires more energy than extracting the less bonded Ni atom of the cluster. In other words, it is easier to dissociate Ni than S atom from the Ni_nS system which suggests that the Ni–S bonding is stronger than the Ni–Ni one. The lowest Ni fragmentation energy corresponds to the extraction of one Ni atom from Ni_4S and the largest desulfurization energy corresponds to the removing the S atom from Ni_3S and Ni_4S. The maximum difference (2.77 eV) between the two energies is obtained for Ni_4S. One can connect the low energy required to dissociate one Ni atom from the Ni_4S cluster to the enlargement of the Ni–Ni inter-atomic distances which takes place upon S-doping of Ni_4 (Fig. 3a). Besides, the apex Ni atom in the trigonal

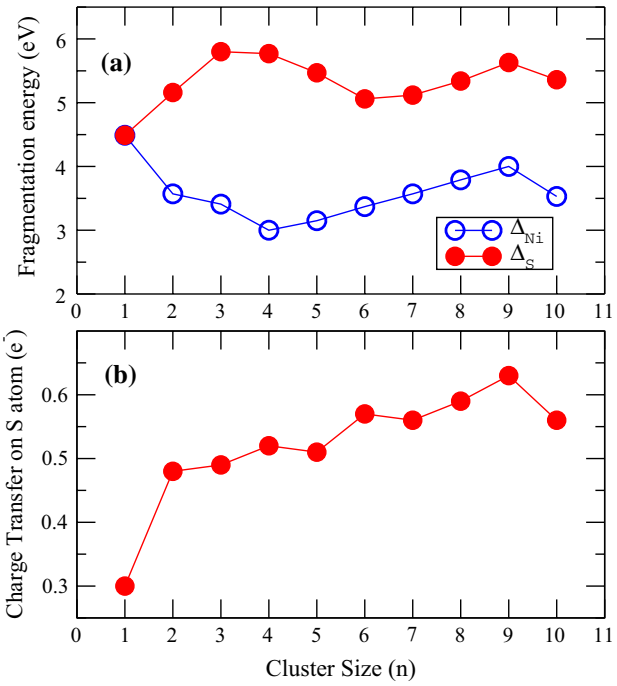

Fig. 4 Fragmentation energies of Ni_nS clusters via the loss of a Ni (Δ_{Ni}) or a S (Δ_S) atom, as a function of cluster size n =1–10 and calculated charge transfer to the sulfur atom in neutral Ni_nS clusters, as function of cluster size n =1–10 (**b**)

bipyramid of Ni_4S is the less-bounded atom due to the repulsion with its Ni neighboring atoms, induced by the charge transfer to the S atom (Fig. 4b).

In order to discuss the relative stability of a cluster of a given size n with respect to its neighboring sizes, we computed the second energy difference, defined as $\Delta_2 E(n) = E(n+1) + E(n-1) - 2E(n)$. This quantity is plotted in Fig. 3b. For S-doped clusters, the most remarkable feature is the noticeable peak at $n = 3$ indicating the high stability of Ni_3S for which the completion of the threefold bonding of S with Ni takes place. Notice that this correlates with the largest desulfurization energy corresponding to the removal of the S atom from Ni_3S. For pure Ni clusters, Ni_6 stands out as particularly stable. As we will see later, these relative stabilities are also reflected in electronic properties like the ionization potential and the electronic affinity.

The vertical ionization potential (VIP) and the vertical electronic affinity (VEA) are important quantities that can be used to characterize the global reactivity of the Ni_nS clusters by means of conceptual DFT indicators [59]. The VIP and VEA for both the pure and doped nickel clusters are plotted in Fig. 5, as a function of cluster size n, where we included the calculated values obtained for the pure Ni_n clusters as well as experimental data reported for them [44, 45]. The VIP (VEA) of Ni_nS clusters is calculated as the energy difference between the neutral clusters and the cationic (anionic) counterparts with the structure of the ground-state neutral cluster. Except the result of Ni atom, for which the difference between the experimental and the calculated values reaches ~ 0.68 eV, the calculated VIPs for Ni_n clusters follow the experimental data [44] rather well as a function of cluster size. This gives further support to our putative ground-state structures. Unfortunately, experimental data concerning VIP and VEA of S-doped nickel clusters are not available so far. However, one can bring out some trends concerning the effect of S-doping on VIP of Ni_nS by comparing their calculated values with those of the pure Ni_n clusters. From Fig. 5, one can see that S-doping produces in general a slight increase of the VIP, except for $n = 2$ and 6. We also note that the VIPs decrease as a function of size in a more monotonic fashion for the S-doped Ni clusters than for the pure ones. As for the calculated values of VEAs for Ni_n clusters, they agree also rather well with the experimental data, except for $n = 3$ for which the difference in the absolute values amounts to 0.28 eV. The VEA of pure Ni clusters increases quite linearly with n between $n = 2$ and 9 and then decreases slightly for $n = 10$. The VEA increases upon S-doping by about 11%. It follows almost the same slope as of pure nickel clusters as a function of cluster size n. The enhancements of both VEA and VIP of S-doped clusters with respect to those of pure Ni_n are consistent with the higher binding energy of the S-doped clusters as compared with the pure ones (Fig. 3c).

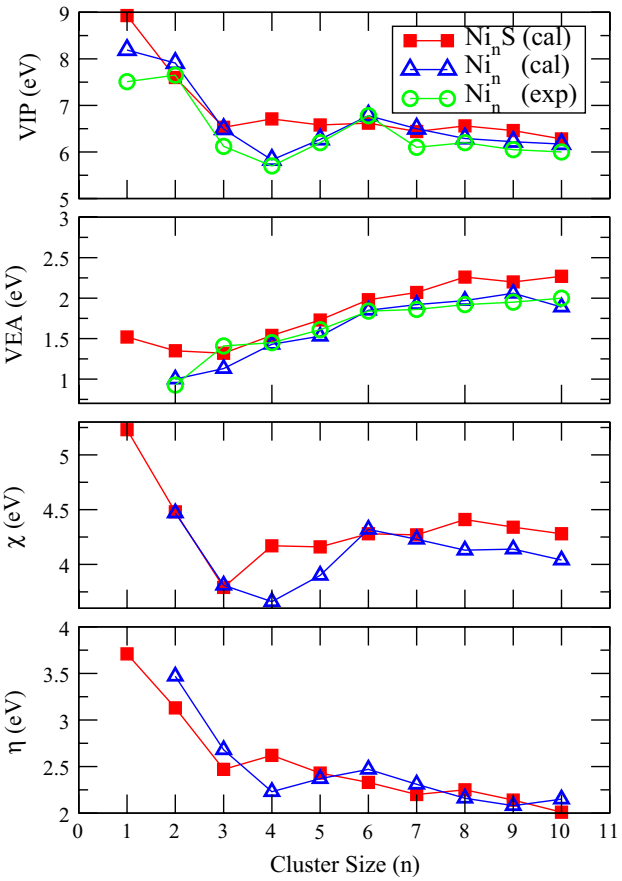

Fig. 5 Vertical ionization potential (VIP), vertical electronic affinity (VEA), electronegativity (χ), and chemical hardness (η) of Ni_n (open triangle) and Ni_nS (filled square) as function of the cluster size n = 1–10

From VIP and VEA, one can evaluate the electronegativity (the negative of the electronic chemical potential μ):

$$\chi = -\mu = \frac{1}{2}(\mathrm{VIP} + \mathrm{VEA}), \tag{5}$$

and the chemical hardness (or fundamental gap, except for a constant factor):

$$\eta = E_{\mathrm{gap}} = \frac{1}{2}(\mathrm{VIP} - \mathrm{VEA}). \tag{6}$$

These quantities are plotted in Fig. 5 as a function of the cluster size n for the pure and doped nickel clusters. Both χ and η of Ni_n clusters display qualitatively the same behavior as the ionization energy as function of the size n. They decrease between $n = 2$ and 4 and then increase up to $n = 6$ after which it decreases again up to $n = 10$. Thus, both quantities present a local maximum at $n = 6$ and a local minimum at $n = 4$ which correlates with the relative high stability of Ni_6 clusters and the low stability of Ni_4 already observed through the second difference in the energy (Fig. 3b). The

electronegativity of S-doped Ni clusters is equal or higher than that of the pure ones. The chemical hardness η does not change much, and the most noticeable change occurs for $n = 4$.

Let us discuss now the magnetic behavior of the pure and S-doped nickel clusters. The total magnetic moment as a function of cluster size n of both sets of clusters is plotted in Fig. 6a. We have also plotted the magnetic moments per atom (Fig. 6b) and included, for the sake of comparison, the available experimental data for pure Ni_n clusters [60]. Our values are smaller than the experimental ones, as it is also the case for almost all ab initio calculations on nickel clusters [26, 33, 35, 40, 42]. Those discrepancies between theory and experiment remain an open question, although the problem may arise from the additional orbital moment contributions or isomerization effects as suggested by some authors [31, 38].

The S-doping of Ni_n clusters affects Ni_6S and Ni_7S by reducing their total moment from 8 μ_B in Ni_6 and Ni_7 to 6 μ_B. We note that for both Ni_6S and Ni_7S clusters, the magnetic state with 8 μ_B is only ~ 0.03 eV higher in energy than the ground state with 6 μ_B. This small effect of S-doping on the total spin polarization of Ni_n clusters is consistent with the weak hybridization between the S and Ni orbitals. To analyze this with two examples, we compare the density of states (DOS) of Ni_5S (Ni_6S) with that of Ni_5 (Ni_6) (Figs. 7, 8). In both cases, the hybridization is weak and involves molecular orbitals far from the Fermi level. For Ni_5S the geometry of the host Ni_5 cluster is essentially preserved (Fig. 1), and no significant rearrangement of both spin-up and spin-down states takes place upon S-doping, the total moment being preserved (Fig. 7). In Ni_6S, however, we observe an important electronic states rearrangement for both spin components upon S-doping (Fig. 8), associated with a structural change. The spectrum rearrangement is accompanied by a spin flip from the majority to minority spin states, giving rise to a decrease of 2 μ_B upon doping.

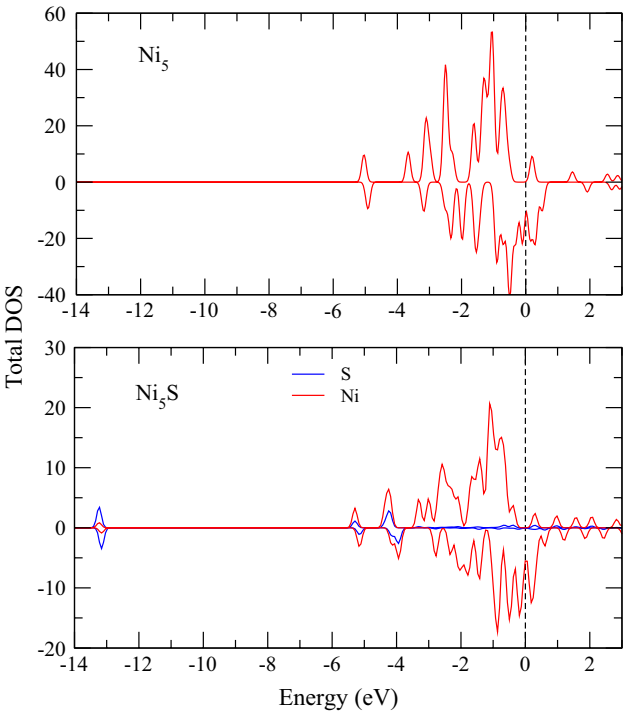

Fig. 7 Total spin-polarized density of states projected on the 5 Ni atoms and on the S atom of the putative ground state of Ni_5S (bottom panel), as compared to the total DOS of the host Ni_5 (top panel). The vertical dashed line indicates the Fermi energy. A Gaussian smearing (0.1 eV) of the states has been used in the plot

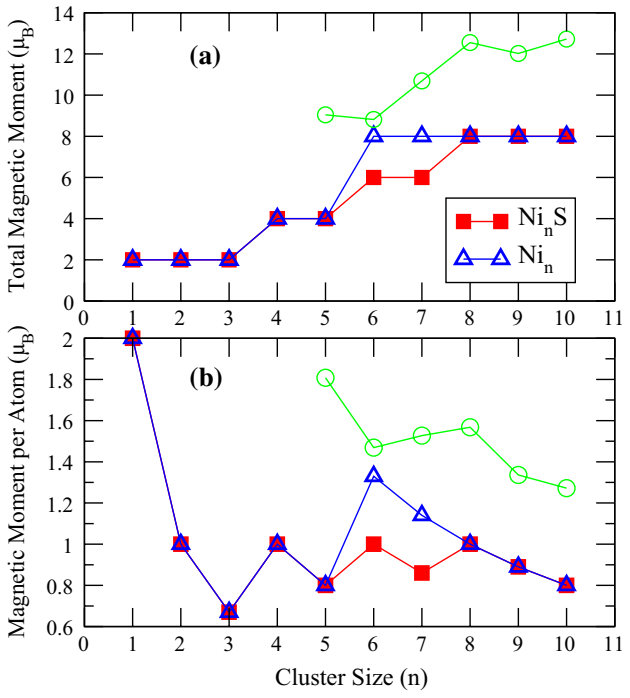

Fig. 6 Total magnetic moments (**a**) and magnetic moments per atom (**b**) of Ni_nS and Ni_n as a function of cluster size n =1–10

Finally, we plot in Fig. 9, as a function of cluster size, the spin-up and spin-down HOMO–LUMO gaps of Ni_nS in their putative lowest-energy structures. The HOMO–LUMO gap of each spin channel is a key quantity for spin-dependent electronic transport at low voltages. The S-doped clusters with $n \leq 4$ and n = 8–10 have relatively large HOMO–LUMO gaps for spin-up states (~ 2.38–1.20 eV), whereas, except for $n = 3$, spin-down states have small gaps (~ 0.60–0.04 eV). The situation is somewhat different for pure Ni_n clusters where the largest HOMO–LUMO gaps for spin-up states are obtained for n = 2–3 and for sizes larger than $n = 5$. Ni_6(Ni_4) displays the largest (lowest) gap 2.46 (0.23 eV) which reflects the high (low) stability of this cluster (Fig. 3b). One can note that the total gap of Ni_4 is the smallest one as reflected in its low stability from the

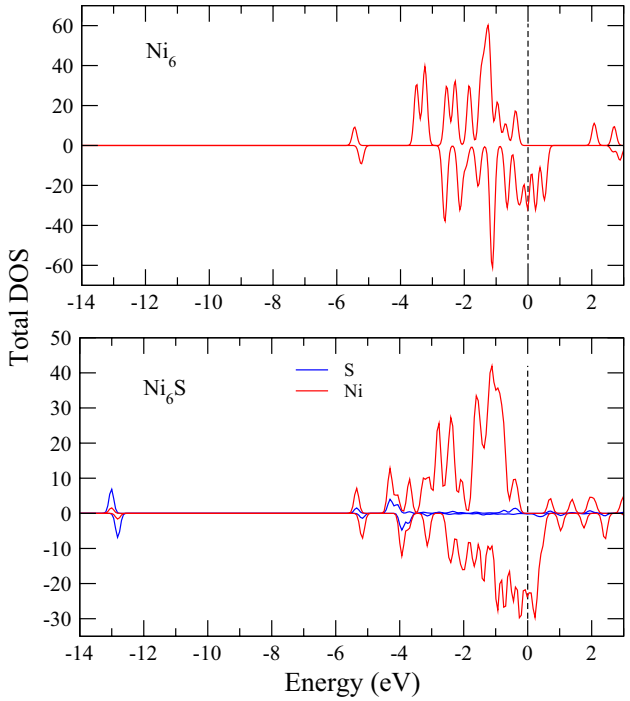

Fig. 8 Total spin-polarized density of states projected on the 6 Ni atoms and on the S atom of the putative ground state of Ni_6S (bottom panel), as compared to the total DOS of the host Ni_6 (top panel). The vertical dashed line indicates the Fermi energy. A Gaussian smearing (0.1 eV) of the states has been used in the plot

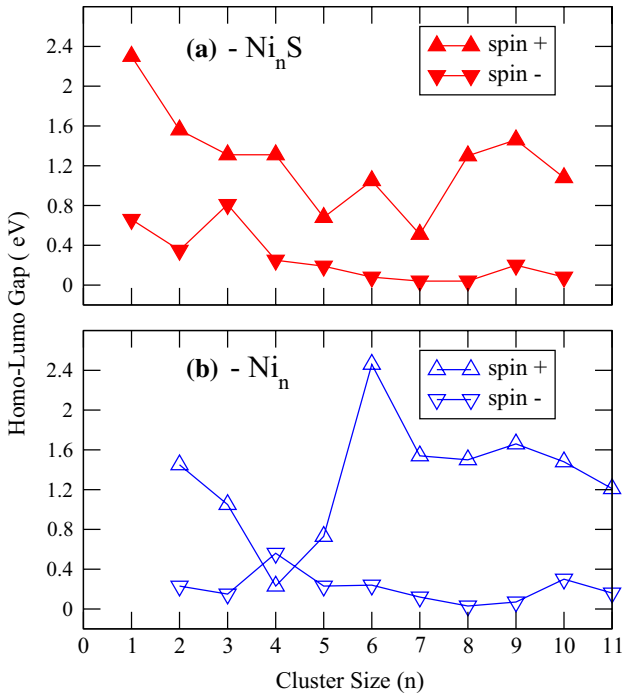

Fig. 9 HOMO–LUMO gap for spin-up and spin-down electrons of Ni_nS (**a**) and Ni_n (**b**) as function of cluster size n =1–10

calculated second differences of energy for pure Ni_n clusters (Fig. 3b). The gaps corresponding to spin-down states are relatively small, and nearly zero for $n > 4$, indicating that these clusters are good candidates as molecular junctions for spin filtering at low bias voltage.

However, the absolute value of the HOMO–LUMO gap has to be taken with care, since it is not a well-defined quantity in DFT that tends to underestimate it due to the lack of electronic correlations. Hybrid functionals such as BLYP, B3LYP, B3PW91, HSE06, among others are designed to better describe part of the exchange and/or correlation effects and, thus, give better absolute values for the HOMO–LUMO gaps than functionals like PBE that otherwise are built from physical grounds and work well for a wide spectrum of properties. To the best of our knowledge, only one theoretical work using B3LYP functional [61] was devoted to nickel sulfide clusters $(NiS)_n$, $n = 3$–5. In order to estimate the discrepancy between the HOMO–LUMO value obtained with PBE and B3LYP, we calculated at the PBE level the ring structure proposed for $(NiS)_3$ in this reference. The PBE HOMO–LUMO gap (0.50 eV) underestimates the B3LYP one (1.04 eV) in about 50%. Other quantities such as ionization potential (IP) and electron affinity (EA) and derived quantities are expected to be less affected since they are obtained as energy differences between ground states calculated at the DFT level, so that they are well-defined indicators within the DFT as opposed to the HOMO–LUMO gap. This is confirmed by the calculated VIPs and VEAs for Ni_n clusters which follow the experimental data rather well as a function of cluster size, as indicated in Fig. 5. For the ring structure proposed for $(NiS)_3$ in reference [61], our calculated values of VIP and VEA, 5.65 and 3.5 eV, respectively, are within 13 and 18% of those of B3LYP, 5 and 4 eV, respectively [61].

4 Conclusions

The main conclusions of our DFT-GGA study of S-doped Ni_nS clusters (n =1–10) can be summarized as follows.

1. The S atom tends to occupy a threefold hollow site, in agreement with DFT calculations [58] of sulfur adsorption on Ni surfaces, which was shown to take place preferentially on the most coordinated sites. A further evidence of the strong S–Ni bonding is provided by the single-atom fragmentation energies: a Ni atom can be extracted from Ni_nS with a lower energy cost than the S atom.
2. S-doping enhances the thermodynamical stability of the Ni clusters. The increase of binding energy upon S-doping is related to the strong S–Ni bonding, also favoured by a partial ionic contribution due to charge

transfer from Ni to S. According to the second differences in energy, Ni_3S is particularly stable with respect to the neighboring sizes. All atoms of this cluster are involved in the threefold bonding, and it has the largest desulfurization energy among the investigated clusters.

3. S-doping only affects the magnetic moment of Ni_6S and Ni_7S by reducing their total moment from 8 μ_B in Ni_6 and Ni_7 to 6 μ_B. The spin-polarized densities of states show a weak hybridization between the S and Ni orbitals, but strong enough structural changes upon doping, in few cases, to produce an electronic states rearrangement consistent with a change of total moment.
4. S-doped clusters with $n \leq 4$ and $n = 8$–10 have relatively large HOMO–LUMO gaps for spin-up states. However, the gaps corresponding to spin-down states are small, and nearly zero for $n > 4$, indicating that most of these clusters are good candidates as molecular junctions for spin filtering at low bias voltage.

Acknowledgements This study was funded by the Algerian Ministry of Higher Education and Scientific Research via the project CNEPRU B00L02UN150120130013 and by the Junta de Castilla y León (Spain) (Project VA124G18).

References

1. Tikhomirov VK, Asatryan K, Galstian TV, Vallee R, Seddon AB (2003) Philos Mag Lett 83:117–124
2. Jain PK, Deepika KS, Saxena NS (2009) Philos Mag 89:641–650
3. Zogg H, Arnold M (2006) Opto Electron Rev 14:33–36
4. Ruxandra V (1997) J Mater Sci Lett 16:1833–1835
5. Li K, Wee ATS, Lin J, Tan KL, Zhou L, Li SFY, Feng ZC, Chou HC, Kamra S, Rohatgi A (1997) J Mater Sci Mater Electron 8:125–132
6. Hartley A, Irvine SJC (2000) J Mater Sci Mater Electron 11:569–573
7. Mane RS, Lokhande CD (2000) Mater Chem Phys 65:1–31
8. Köckerling M, Johrendt D, Finckh EW (1998) J Am Chem Soc 120:12297
9. Chevrel R, Hirrien M, Sergent M (1986) Polyhedron 5:87
10. Stiefel EI, Matsumoto K (1996) ACS Symp Ser 653:2
11. Krebs B, Henkel G (1991) Angew Chem Int Ed Engl 30:769
12. Harris S, Chianelli RR (1984) J Catal 86:400
13. Prins R, de Beer VHG, Somorjai GA (1989) Catal Rev Sci Eng 31:1
14. Paskach TJ, Schrader GL, McCarley RE (2002) J Catal 211:285
15. Mlynarski P, Salahub DR (1991) J Chem Phys 95:6050
16. Jellinek J, Garzón IL (1991) Z Phys D 20:239
17. Stave MS, DePristo AE (1992) J Chem Phys 20:3386
18. Garzón IL, Jellinek JJ (1992) In: Jena P, Khanna SN, Rao BK (eds) Physics and chemistry of fine systems, from clusters to crystals, vol 1. Kluwer Academic, Dordrecht, p 405
19. López MJ, Jellinek J (1994) Phys Rev A 50:1445
20. Menon M, Connolly J, Lathiotakis N, Andriotis A (1994) Phys Rev B 50:8903
21. Lathiotakis NN, Andriotis AN, Menon M, Connolly J (1996) J Chem Phys 104:992
22. Bouarab S, Vega A, Lopéz MJ, Iñiguez MP, Alonso J (1996) Phys Rev B 55:13279
23. Castro M, Jamorski C, Salahub DR (1997) Chem Phys Lett 271:133
24. Reuse F, Khanna SN (1995) Chem Phys Lett 234:77
25. Nayak SK, Rao BK, Jena P (1997) J Phys Chem A 101:1072
26. Reddy BV, Nayak SK, Khanna SN, Rao BK, Jena P (1998) J Phys Chem A 102:1748
27. Doye JPK, Wales DJ (1998) New J Chem 22:733
28. Curotto E, Matro A, Freeman DL, Doll JD (1998) J Chem Phys 108:729
29. Michaelian K, Rend N, Garz IL (1999) Phys Rev B 60:2000
30. Xiang Y, Sun DY, Gong XG (2000) J Phys Chem A 104:2746
31. Khanna SN, Beltran M, Jena P (2001) Phys Rev B 64:235419
32. Michelini MC, Pis Diez R, Jubert AH (2001) Int J Quantum Chem 85:22
33. Duan HM, Gong XG, Zheng QQ, Lin HQ (2001) J Appl Phys 89:7308
34. Luo CL (2002) Mater Sci Eng 10:13
35. Ashman C, Khanna SN, Pederson MR (2003) Chem Phys Lett 368:257
36. Grigoryan VG, Spingborg M (2004) Phys Rev B 70:205415
37. Xie Z, Ma QM, Liu Y, Li YC (2005) Phys Lett A 342:459
38. Aguilera-Granja JM, Montejano-Carrizales RA, Guirado-Lpez RA (2006) Phys Rev B 73:115422
39. Deshpandre MD, Roy S, Kanhere DG (2007) Phys Rev B 76:195423
40. Yao YH, Gu X, Ji M, Gong XG, Wang DS (2007) Phys Lett A 360:629
41. Lee B, Lee GW (2007) J Chem Phys 127:164316
42. Lu QL, Luo QQ, Chen LL, Wan JG (2011) Eur Phys J D 61:389
43. Chikhaoui A, Haddab K, Bouarab S, Vega A (2011) J Phys Chem A 115:1399714005
44. Knickelbein MB, Yang S, Riley SJ (1990) J Chem Phys 93:94
45. Rienstra-Kiracofe JC, Tschumper GS, Schaefer HFIII, Nandi S, Ellison GB (2002) Chem Rev 102:231
46. Kresse G, Hafner J (1993) Phys Rev B 47:558
47. Perdew JP, Burke K, Ernzerhoh M (1996) Phys Rev Lett 77:3865–3868
48. Henkelman G, Arnaldsson A, Jónsson H (2006) Comput Mater Sci 36:354–360
49. Sanville E, Kenny SD, Smith R, Henkelman G (2007) J Comput Chem 28:899–908
50. Tang W, Sanville E, Henkelman G (2009) J Phys Condens Matter 21:084204–7
51. Tazibt S, Chikhaoui A, Bouarab S, Vega A (2017) J Phys Chem A 121:3768–3780
52. Vaidya N, Indian J (1976) Pure Appl Phys 14:600
53. Pinegar JC, Langenberg JD, Arrington CA, Spain EM, Morse MD (1995) Chem Phys 102:666
54. Wang H, Haouari H, Craig R, Lombardi JR, Lindsay DM (1996) J Chem Phys 104:3420
55. Ahmed F, Nixon ER (1979) J Chem Phys 71:3547
56. Soler JM, Artacho E, Gale JD, Garca A, Junquera J, Ordejon P, Sanchez-Portal D (2002) J Phys Condens Matter 14:2745
57. Ordejon P, Artacho E, Soler JM (1996) Phys Rev B 53:R10441
58. Kandaskalov D, Monceau D, Mijoule C, Damien (2013) Surf Sci 617:15–21
59. Geerlings P, De Proft F, Langenaeker W (2003) Chem Rev 103:1793–1873
60. Apsel SE, Emmert JW, Deng J, Bloomfield LA (1996) Phys Rev Lett 76:1441
61. Nagarajan V, Chandiramouli R, Sriram S, Gopinath P (2014) J Nanostruct Chem 4:87